LDA Combined Depth Similarity and Gradient Features for Human Detection using a Time-of-Flight Sensor

Alexandros Gavriilidis, Carsten Stahlschmidt, Jörg Velten and Anton Kummert
Faculty of Electrical Engineering and Media Technologies, University of Wuppertal, D-42119 Wuppertal, Germany

Keywords: Human Detection, Depth Image Features, LDA Feature Combination, Video Processing.

Abstract: Visual object detection is an important task for many research areas like driver assistance systems (DASs), industrial automation and various safety applications with human interaction. Since detection of pedestrians is a growing research area, different kinds of visual methods and sensors have been introduced to overcome this problem. This paper introduces new relational depth similarity features (RDSF) for the pedestrian detection using a Time-of-Flight (ToF) camera sensor. The new features are based on mean, variance, skewness and kurtosis values of local regions inside the depth image generated by the Time-of-Flight sensor. An evaluation between these new features, already existing relational depth similarity features using depth histograms of local regions and the well known histogram of oriented gradients (HOGs), which deliver very good results in the topic of pedestrian detection, will be presented. To incorporate more dimensional feature spaces, an existing AdaBoost algorithm, which uses linear discriminant analysis (LDA) for feature space reduction and new combination of already extracted features in the training procedure, will be presented too.

1 INTRODUCTION

Conventional camera systems capturing only available light of the surrounding area have many benefits as well as drawbacks for the task of visual pedestrian detection. Benefits of passive camera systems are, beside the financial point, the usability for many different tasks, like pattern recognition, object detection and image registration. The lighting conditions are the strongest limitation factors for conventional camera systems. Relating to pedestrian detection, the appearance, e.g. color of clothes, and the contrast of the pedestrian to the background are typical problems for conventional monocular (Enzweiler and Gavrila, 2009) or stereo (Keller et al., 2011) camera systems. Besides cues for detection of pedestrians which are exhaustive evaluated in (Dollár et al., 2012), information about the distance to a detected object are essential for many assistance systems. The estimation of a distance to a detected object based on camera calibration and conventional monocular camera systems is a typical problem too. To overcome such problems, sensors like Time-of-Flight (ToF) cameras, also called RGB-D cameras, can be used. In (Ikemura and Fujiyoshi, 2010) relational depth similarity features (RDSFs) for the detection of pedestrians have been introduced, which are extracted from a depth image captured by a TOF camera. Based on a maximum range resolution of $7.5m$ of the TOF camera, a depth image will be quantized into 25 bins, whereupon each bin has a range resolution of $0.3m$. For a rectangular region, the depth histogram will be created using the occurrence of pixel inside each bin of the 25 quantization steps. After normalization of the histogram, the Bhattacharyya distance between two different rectangular regions inside the image will be calculated and the scalar result will be used as feature for an AdaBoost classifier. The time of computing the 25 integral images, as well as the evaluation of the Bhattacharyya distance over two 25-dimensional histograms for many different rectangular region combinations can be very expensive.

Another approach like (Mattheij et al., 2012) evaluates the well known Haar-like features from (Viola and Jones, 2001b) on depth images and shows that Haar-like features can deliver accurate results combined with a fast calculation time using integral images. Histogram of Depth Differences (HDD) developed in (Wu et al., 2011) and derived from the Histogram of Oriented Gradients (HOGs) (Dalal and Triggs, 2005) is nearly the same. The only difference is the use of the whole 360 degrees of the possible orientations and not just the 180 degrees as described in (Dalal and Triggs, 2005) of the HOG feature.

Gavriilidis A., Stahlschmidt C., Velten J. and Kummert A..
LDA Combined Depth Similarity and Gradient Features for Human Detection using a Time-of-Flight Sensor.
DOI: 10.5220/0005257403490356
In *Proceedings of the 10th International Conference on Computer Vision Theory and Applications* (VISAPP-2015), pages 349-356
ISBN: 978-989-758-089-5

In (Spinello and Arras, 2011) the Histogram of Oriented Depths (HOD) feature will be introduced, that has been also derived from the HOG feature. The HOD will be calculated in the depth image and used by a soft linear support vector machine (SVM) to detect pedestrians. To improve the decision of the HOD, a so called Combo-HOD will be introduced that uses two detectors trained each on either the depth image with HOD features or the intensity (grayscale) image with HOG features and combines in that case the sensor cues of each image. The Combo-HOD promises more accurate precision than the single detectors on either the depth or the RGB image.

Based on the idea of local binary pattern (LBP), in (Wang et al., 2012) so called pyramid depth self-similarities (PDSS) are introduced, which will be used with a depth image. The core part is to compare local areas in the manner of LBP features, e.g. to compare a cell (an image area) of a detection window with its neighbouring cells, by use of histogram intersection methods. To concatenate the histograms by a spatial pyramid over the depth image is a time consuming task too. To be as fast and accurate as possible, the presented approach of this paper is based on features which are also comparing the relation in depth of two different areas, but can be computed very fast, like Haar-like features. Time consuming features can be used to increase the performance in addition to the weak features, which will be introduced later in this paper.

The remainder of the paper is structured as follows, the next section gives an overview of the used sensor, the available sensor data and other basic reflections regarding the difference between intensity and depth images. The available features for pedestrian detection in $2.5D$ (RGB-D) data will be described in section three. Section four describes the used classifier and the usage of high dimensional features by linear discriminant analysis (LDA) transformation. The following section show up the results of the paper and in the last section, a summary and conclusions will be given.

2 PRELIMINARY CONSIDERATIONS

The used ToF camera is the CamCube 3.0 from PMD Technologies GmbH with a maximum measurement range of up to $7.5m$ for the available depth image. Field of view of the ToF camera is 40 degrees in both directions with a pixel resolution of (200×200) by a possible frame rate of over 30 frames per second (fps). A general image can be described by pixel values $g = f(\mathbf{n})$ with $f : \mathbf{n} \rightarrow g, g \in \mathbb{R}, \mathbf{n} \in \mathcal{M}$, where

$$\mathcal{M} = \{\mathbf{n} \in \mathbb{Z}^m | \mathbf{0} \leq \mathbf{n} < \mathbf{N}\} \tag{1}$$

and $\mathbf{N} \in \mathbb{Z}^m$ describing the number of values in all dimensions of an image $f(\mathbf{n})$, $\mathbf{0}$ is a vector containing only zeros. The used ToF camera delivers three important two dimensional (2D) images with $\mathbf{n} = [n_u, n_v]^T$ including an intensity image $I(n_u, n_v) \in [0, 255]$, a depth image $\mathcal{D}(n_u, n_v) \in \mathbb{R}^{\geq 0}$ and an amplitudes image $\mathcal{A}(n_u, n_v) \in \mathbb{N} \backslash \{0\}$, whereupon each image has the same pixel resolution of $\mathbf{N} = [200, 200]^T$ pixel. In other words, one great property of the Photonic Mixer Device (PMD) sensor is, there are three images available and each pixel has three representations, which can be used for new feature combinations. The amplitudes image, which will be not presented in this scope, includes information about the signal strength of the measured reflected light. It could be used as indicator for accurate measured depth information. In Figure 1 the intensity and the depth image can be seen. The intensity image of the PMD camera can be badly scaled, based on poor reflected light. Because of this, some areas will deliver very poor gradient information, like it can be seen in the lower part of the intensity image of Figure 1. In contrast to this, the depth image will deliver small gradients, if all observed objects are close to the same plane, e.g. an object close to a wall. Additionally, a huge problem of the depth image of the ToF camera is the ambiguity in the distance resolution, which causes gradients in the depth image that are not induced by real objects. But for objects up to $7.5m$, the depth image can deliver accurate gradients along the borders of objects segmented by the surrounding area. This illumination resistant property of the ToF camera and the information about the measured distance of an object to the sensor in the real world can be used to create new features by combination of existing ones to improve the object detection task.

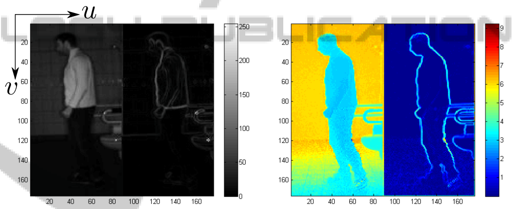

Figure 1: On the left hand side the intensity image and the corresponding magnitude image of the gradient calculation, as described in section 3, are shown. On the right hand side, the depth image is presented as well as the corresponding magnitudes image.

3 FAST DEPTH RELATIONAL SIMILARITY FEATURES

Based on the work of (Ikemura and Fujiyoshi, 2010) new fast features, which are described in the following subsections, will be inspired to detect humans in a depth image of a ToF camera. Since, the RDSFs developed in (Ikemura and Fujiyoshi, 2010) describe how two rectangular regions inside the depth image are similar to each other based on a quantized depth histogram, it is also possible to describe such a relation based on the idea of (Mattheij et al., 2012). The idea is to remove the bottlenecks of the RDSF calculation, which are based on the calculation of 25 integral images and the calculation of the Bhattacharyya distance between two 25-dimensional feature vectors, but to keep the smart combination of two different local regions inside the image plane. Based on the training size of an image of (64×128) pixel, the smallest size of a region (cell) is assumed as (8×8) pixel, like described in (Ikemura and Fujiyoshi, 2010), and each region can grow along one image dimension about its smallest cell size. Since, a region should not reach the size of the whole training window, the largest size of one region will be limited to (48×96) pixel. Each region between (8×8) pixel and (48×96) pixel, including the extremal values (48×8) pixel and (8×96) pixel, will be shifted by one pixel inside the training image. Since, the number of all possible combinations between two different regions shifted pixel by pixel will be too large, one of both regions will not change the size and position. The choice of this assumption will be discussed in the next sections. The remaining number of possible features is now 49248, whereupon one region will not be changed. In contrast to this, the regions described in (Ikemura and Fujiyoshi, 2010) are growing in both image directions with the smallest cell size at the same time, in other words quadratically, and only regions on the current grid, which is defined by the smallest cell size, are used. Each combination between two regions on this grid leads to a total number of 120.786 possible features, as described in (Ikemura and Fujiyoshi, 2010).

3.1 Mean and Variance Features (MV-RDSF)

Inspired by the idea of (Ikemura and Fujiyoshi, 2010) to compare the depth information between two rectangular regions inside of the depth image and due to a pedestrian will have distances which are close to one plane, the comparison of mean and variance values of two regions can be used as feature to find characteristics of a pedestrian. Because of each combination between two different regions in an image of (64×128) pixel resolution will lead to an exorbitant number of possible features, as described at the beginning of this section, the following assumption will be preferred. Based on an empirical evaluation of all possible combinations of two rectangular regions, a region on the upper part of the body is one of the best choices for one of both rectangular regions which should not be changed anymore. This first rectangular region is placed on the left upper corner $\mathbf{n} = [24, 32]^T$ with a width of 16 pixel and a height of 32 pixel. In Figure 2, three different selected feature combinations can be seen, whereupon the green (middle) rectangle does not change its size or position, only by scaling, as all the other rectangles too. The integral image representation can be used to be more efficient by calculating the local mean

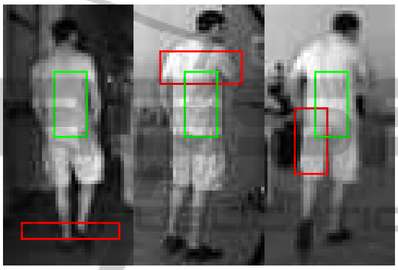

Figure 2: Three different selected mean and variance features which has been selected during the AdaBoost training. The green rectangle (each time on the torso of the human) is the same feature in each boosting iteration.

$$\mu(u,v,w,h) = \frac{1}{w \cdot h} \sum_{i=u}^{w} \sum_{j=v}^{h} \mathcal{D}(i,j), \qquad (2)$$

and the local variance

$$E\left\{(X-\mu)^2\right\} = \sigma(u,v,w,h)^2 = \frac{1}{w \cdot h}\left(\sum_{i=u}^{w}\sum_{j=v}^{h}\mathcal{D}(i,j)^2\right) - \mu^2, \qquad (3)$$

as defined in (Shafait et al., 2008), where (u,v,w,h) are the image coordinates, width and height of a rectangular region. In other words, two integral images, one over the normal depth image and one over the squared depth image, can be used to calculate the mean and the variance of a rectangular region using the integral image representation. The two dimensional feature vector will be the difference

$$\mathbf{x} = \begin{pmatrix} \|\mu_1 - \mu_2\| \\ \|\sigma_1^2 - \sigma_2^2\| \end{pmatrix} \qquad (4)$$

of the means (μ_1, μ_2) and the variances (σ_1^2, σ_2^2) of the two regions. This simple $2D$ feature can be used to describe the difference of depth between two rectangular regions.

3.2 Mean, Variance, Skewness and Kurtosis Features (MVSK-RDSF)

Besides the mean and variance of depth image information between two rectangular regions, it is possible to extend the feature vector of the last subsection by the two values skewness and kurtosis. The skewness

$$E\left\{\left(\frac{X-\mu}{\sigma}\right)^3\right\} = \mathrm{skew}(u,v,w,h) = \frac{1}{\sigma^3}\left(\frac{1}{w\cdot h}\left(\sum_{i=u}^{w}\sum_{j=v}^{h}\mathcal{D}(i,j)^3\right) - \frac{3\mu}{w\cdot h}\left(\sum_{i=u}^{w}\sum_{j=v}^{h}\mathcal{D}(i,j)^2\right) + 2\mu^3\right) \tag{5}$$

and the kurtosis

$$E\left\{\left(\frac{X-\mu}{\sigma}\right)^4\right\} = \mathrm{kurt}(u,v,w,h) = \frac{1}{\sigma^4}\left(\frac{1}{w\cdot h}\left(\sum_{i=u}^{w}\sum_{j=v}^{h}\mathcal{D}(i,j)^4\right) - \frac{4\mu}{w\cdot h}\left(\sum_{i=u}^{w}\sum_{j=v}^{h}\mathcal{D}(i,j)^3\right) + \frac{6\mu^2}{w\cdot h}\left(\sum_{i=u}^{w}\sum_{j=v}^{h}\mathcal{D}(i,j)^2\right) - 3\mu^4\right) \tag{6}$$

can be used in this representation also with integral images. The combined four dimensional feature vector is then based on

$$\mathbf{x} = \begin{pmatrix} ||\mu_1 - \mu_2|| \\ ||\sigma_1^2 - \sigma_2^2|| \\ ||\mathrm{skew}_1 - \mathrm{skew}_2|| \\ ||\mathrm{kurt}_1 - \mathrm{kurt}_2|| \end{pmatrix} \tag{7}$$

and includes some more information about the distributions of depth values between the both regions.

3.3 Mean, Variance and HOG Features (MV-HOG-RDSF)

Since, the MV-RDSF and MVSK-RDSF representations might not be efficient enough to distinguish a pedestrian from all other objects, the combination of the relation of depth and depth gradients can be used. Therefore, the idea of the HOG feature representation can be used applied on the depth image. Since, one of both rectangular regions (green region of Figure 3) does not include any gradient in the depth image, if a pedestrian is visible like shown in Figure 2, the gradient calculation will only be used on the second region (red region). Because of, only one region is available, the original HOG representation with one cell will be used as the whole HOG block. The HOG feature will be calculated with the integral image representation based on the gradient images, calculated by convolving the depth image with the masks $[1,0,-1]$ and $[-1,0,1]^T$, and the magnitude between the gradients in both image directions. Finally, each HOG block will be normalized using the $L1$-norm. For the evaluation, five bins have been used for one HOG feature, which can be seen in Figure 3. The final MV-HOG-RDSF is a concatenation of the two dimensional MV-RDSF and the HOG feature, as it can be seen on the right hand side of Figure 3. This new feature representation includes the relation in depth direction between two rectangular regions and the gradient information in depth direction from the rectangular region, which is changing its size and position (red rectangle).

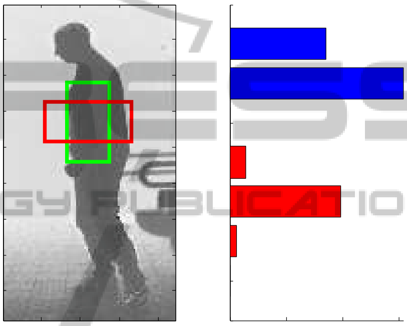

Figure 3: One feature combination between two rectangles can be seen on the left hand side. On the right hand side, the corresponding feature vector with concatenated mean, variance and HOG values. The first two bars (coloured in blue) are the mean and variance differences, the values from three to seven are the histogram values of the red coloured rectangle, which can change in size and position, as shown in Figure 2.

4 CLASSIFIER

Fast and accurate detection of objects depends on the underlying feature space and the used classifier. As classifier for pedestrian detection, the SVM will be used in many applications due to the usage of high dimensional feature spaces. Because of the feature space of a pedestrian classifier can be highly non-linear, the classes pedestrian and non-pedestrian may not be sufficiently dividable by a linear SVM kernel. Therefore, boosting classifiers such as AdaBoost (Viola and Jones, 2001a) or non-linear kernels with a SVM can be used. Non-linear SVM evaluation is very expensive, but on the other side also very accurate. Based on the property of fast detection, the asymmetric cascaded AdaBoost will be used in this paper as described in (Viola and Jones, 2001a).

To improve the usage of presented features of the last section, the combination and extraction of features based on the linear discriminant analysis (LDA) will be used as presented in (Nunn et al., 2009). A training set can be defined like

$$\underbrace{(y_1,\mathbf{x}_1),\ldots,(y_{M_p},\mathbf{x}_{M_p})}_{\text{positive examples}},\underbrace{(y_{M_p+1},\mathbf{x}_{M_p+1}),\ldots,(y_M,\mathbf{x}_M)}_{\text{negative examples}}$$

with $M_p, M \in \mathbb{N}\backslash\{0\}$ and label information $y_i \in \{-1,1\}$, where $i = 1,\ldots,M$, for positive $(y_i = +1)$ and for negative $(y_i = -1)$ training examples. For each example of the training set with a feature vector

$$\mathbf{x}_i = (x_1,\ldots,x_m)^T, m \in \mathbb{N}\backslash\{0\} \tag{8}$$

the AdaBoost algorithm uses weights

$$D_{t+1}(i) = \frac{D_t(i)e^{(-\alpha_t y_i h_t(\mathbf{x}_i,f,p,\Theta))}}{Z_t}, \tag{9}$$

with $t \in \mathbb{N}\backslash\{0\}$, $D_1(i) = \frac{1}{M}$ and Z_t as normalization factor to keep D_{t+1} as a distribution for all training examples. The value α_t will be calculated using the minimum error

$$\varepsilon_t = \min_{f,p,\Theta}\sum_i D_t(i)\,|h_t(\mathbf{x}_i,f,p,\Theta) - y_i| \tag{10}$$

of the weak classifiers

$$h_t(\mathbf{x}_i,f,p,\Theta) = \begin{cases} 1 & \text{if } pf(\mathbf{x}_i) < p\Theta \\ -1 & \text{otherwise} \end{cases} \tag{11}$$

where p is a sign for the inequality, $f(\mathbf{x}_i)$ is the result of the feature evaluation and Θ is a threshold value, which has to be determined. Based on the error ε_t, which will be evaluated for each round of boosting in the training phase, the value

$$\alpha_t = \log\left(\frac{1-\varepsilon_\mathrm{t}}{\varepsilon_\mathrm{t}}\right) \tag{12}$$

can be calculated. Each feature vector can be transformed into one linear dimension by

$$\tilde{x}_i = \mathbf{w}^T \cdot \mathbf{x}_i \tag{13}$$

where $\mathbf{w}$ is the transformation vector determined from

$$\mathbf{w} = \boldsymbol{\Sigma}^{-1}(\boldsymbol{\mu}_1 - \boldsymbol{\mu}_2) \tag{14}$$

with $(\boldsymbol{\mu}_1, \boldsymbol{\mu}_2)$ as the means of the class one and class two in a two class problem. The matrix $\boldsymbol{\Sigma}$ is the covariance matrix of both classes as defined in (Nunn et al., 2009) and (Izenman, 2008). All AdaBoost weights $D_t(i)$ have to be considered in the calculation of the covariance matrix $\boldsymbol{\Sigma}$. Therefore, the means

$$\boldsymbol{\mu}_1 = \frac{1}{\sum_{i=1}^{N_p} D_t(i)}\sum_{i=1}^{N_p} D_t(i)\cdot\mathbf{x}_i, \tag{15}$$

$$\boldsymbol{\mu}_2 = \frac{1}{\sum_{i=N_p+1}^{N} D_t(i)}\sum_{i=N_p+1}^{N} D_t(i)\cdot\mathbf{x}_i \tag{16}$$

will be used to calculate the covariance matrices of the different classes

$$\boldsymbol{\Sigma}_1 = \frac{1}{\sum_{i=1}^{N_p} D_t(i)}\sum_{i=1}^{N_p} D_t(i)\cdot(\mathbf{x}_i - \boldsymbol{\mu}_1)(\mathbf{x}_i - \boldsymbol{\mu}_1)^T, \tag{17}$$

$$\boldsymbol{\Sigma}_2 = \frac{1}{\sum_{i=N_p+1}^{N} D_t(i)}\sum_{i=N_p+1}^{N} D_t(i)\cdot(\mathbf{x}_i - \boldsymbol{\mu}_2)(\mathbf{x}_i - \boldsymbol{\mu}_2)^T \tag{18}$$

and the combined covariance matrix

$$\boldsymbol{\Sigma} = \boldsymbol{\Sigma}_1 + \boldsymbol{\Sigma}_2, \tag{19}$$

respectively.

Each of the features, described in the last section 3, will be transformed by the LDA transformation to calculate the result of the weak classifiers for the AdaBoost training. It is worthwhile to know, that with this LDA transformation it is possible to combine the MV-RDSF and the classical HOG features into one new feature space. The transformation vector $\mathbf{w}$, which transforms the current feature, will be selected in the training procedure. The combination of selected transformation vectors and features will be used to classify in the online procedure an unknown feature vector for the AdaBoost classifier.

5 EVALUATION

5.1 Database

The RDSF of (Ikemura and Fujiyoshi, 2010), the new MV-RDSF, MVSK-RDSF, the combined MV-HOG-RDSF and the classic HOG features will be trained with an asymmetric AdaBoost algorithm and evaluated over a generated dataset including $8400, 3600$ positive and $6650, 2850$ negative examples for training and testing, respectively. Some positive and negative examples of depth images can be seen in Figure 4. Due to the detection of occluded humans, as it is

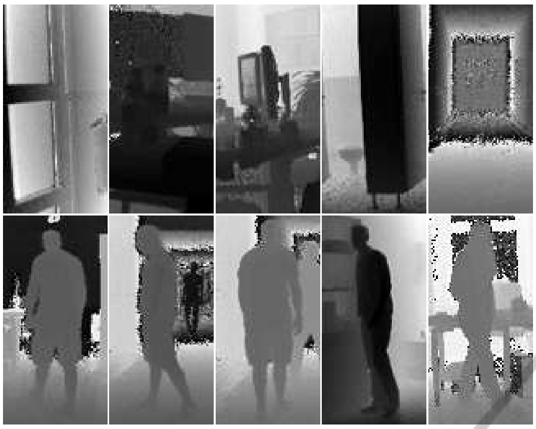

Figure 4: The upper part of the figure includes negative examples of the training and test set and the lower part of the figure shows some positive examples.

described in (Ikemura and Fujiyoshi, 2010), is not in focus of this evaluation, the positive examples include only small partial occlusion from the foreground and a large variation of the background, including also ambiguities in the depth caused by the time of flight principle.

5.2 Feature Performance Comparison

The evaluated classical HOG features contain one cell ((8×8) pixel) per block to be comparable to the new combined MV-HOG-RDSF. Each possible rectangular region from (8×8) pixel up to (56×112) pixel with an increasing factor of 8 pixel in each dimension of the block will be considered. Additionally, each possible HOG block will be shifted by one pixel over the whole training window, as described also in section 3, and not by the smallest cell size as it will be done by the RDSFs. This results in a total number of 48510 classical HOG features.

Figure 5 shows the results of the trained classifiers with the new features based on mean, variance, skewness and kurtosis. The mean and variance features (MV-RDSF) deliver the worst performance. By extending the MV-RDSF with skewness and kurtosis properties, it is possible to increase the performance of the classifier only slightly. However, both features, the MV-RDSF and the MVSK-RDSF, cannot reach the performance of the original RDSF, because the feature space is strongly limited for a good separation. Strong noise involved by the depth ambiguity and the sensor hardware cannot be considered just by the mean and variance of depth information.

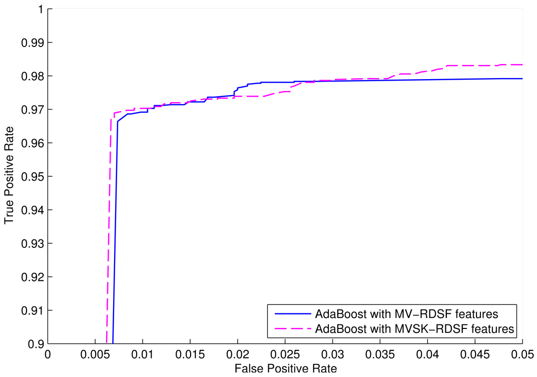

Figure 5: The receiver operating characteristics (ROCs) of the MV-RDSF and MVSK-RDSF trained with the asymmetric AdaBoost procedure.

The comparison between the classical HOG feature and the RDSF of (Ikemura and Fujiyoshi, 2010) is shown in Figure 6. The classical HOG feature has similar results as the RDSF of (Ikemura and Fujiyoshi, 2010). Again, it is mentionable that in (Ikemura and Fujiyoshi, 2010) it is not described which version of a HOG feature has been used. Here, as described in section 3, one HOG block consists of one cell with the size of (8×8) pixel and has only 5 orientations. The concatenation of the MV-RDSF and the HOG features, the MV-HOG-RDSF, uses a combination of similarity in depth and depth gradients for shape characterization and delivers the best results in the experiments, as it can be seen in Figure 6. Based on the LDA transformation of the combined depth relation and depth gradients, more information for the separation of positive and negative examples are available. On the other hand, the computation of the integral images for the orientations of the classical HOG feature and the integral images over the mean and variance of the depth image is still faster than the generation of 25 integral images to quantize the depth image as used by (Ikemura and Fujiyoshi, 2010). Furthermore, the calculation of the MV-HOG-RDSF in the online detection phase is still faster than the computation of the RDSF, because for each RDSF the

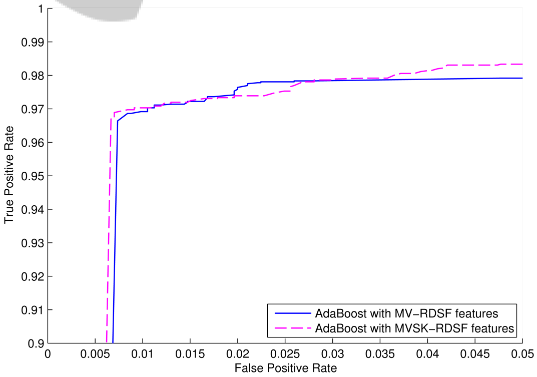

Figure 6: The receiver operating characteristics (ROCs) of the classical HOG feature, the RDSF and the MV-HOG-RDSF trained with the asymmetric AdaBoost procedure.

Bhattacharyya distance of two 25 dimensional vectors has to be determined. This improvement in speed and the better performance in detection favour the usage of the MV-HOG-RDSF for the human detection in depth images, where strong occlusion of the humans has not to be considered.

Each classifier has been trained with a final false positive rate of 1%. To compare the performance of the different features, the 1% false positive point on the ROC curves will be used. Table 1 includes the results of the ROC curves in this point for each feature used with the asymmetric AdaBoost classifier. The MV-RDSF and MVSK-RDSF are significantly inferior to the RDSF, but the combination of gradients features and depth features deliver an improved detection accuracy.

Table 1: The table inlcudes the results of the different features at the 1% false positive point on the ROC curves. The last column shows the number of selected features of the final classifier which has been selected during the training phase.

Feature	True Positive Rate	Number of Features
MV-RDSF	0.9703	73
MVSK-RDSF	0.9703	103
MV-HOG-RDSF	0.9867	24
Classic HOG	0.9811	33
RDSF	0.9828	41

5.3 Relative Time Performance

However, the gap in the performance is not so large, but the time complexity of the feature and integral image calculation between the RDSF and the MV-HOG-RDSF is huge. The calculation of the integral images of the MV-HOG-RDSF is twice as fast as of the RDSF, without pronouncing the absolute time values, which are hardware dependent. It is worthwhile to know, no parallelization has been used for each computation. Additionally, the single feature calculation of the MV-HOG-RDSF is also still faster than the calculation of the Bhattacharyya distance between two 25 dimensional feature vectors.

Furthermore, the computational costs of the final classifiers are directly dependent from the number of selected features in the training procedure. As it can be seen in Table 1, the MV-RDSF and MVSK-RDSF have many selected features in the final classifier, but are still very fast due to the simplicity of the used features. The new MV-HOG-RDSF have just almost half of the number of selected features for the final classifier as the RDSF and also less selected features than the classical HOG features. The reduced number of selected features and the low computational complexity of the MV-HOG-RDSF in relation to the RDSF

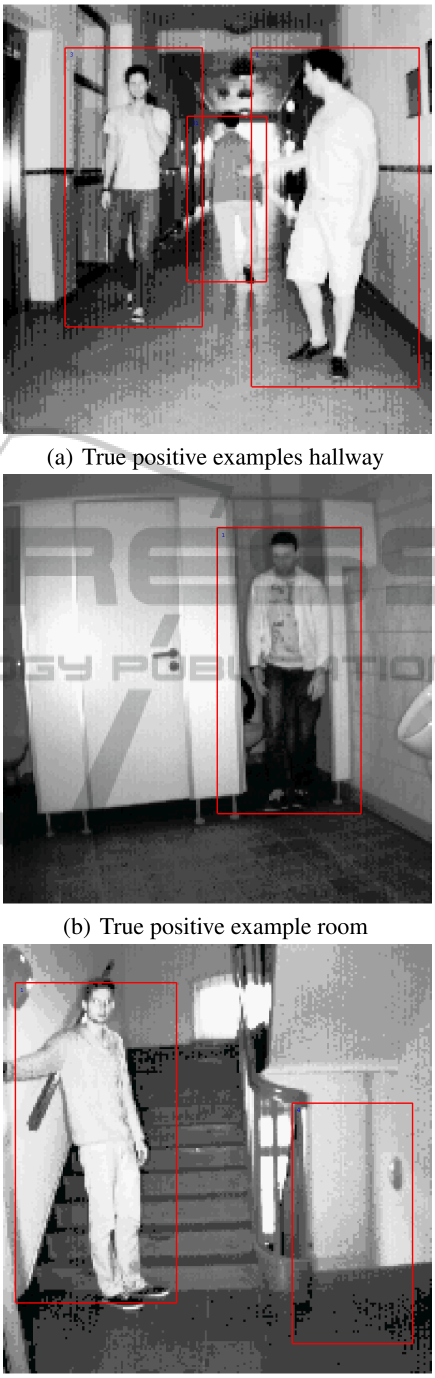

(a) True positive examples hallway

(b) True positive example room

(c) True and false positive examples

Figure 7: Subfigure 7(a) shows some true positive results of the MV-HOG-RDSF classifier in a hallway, where depth ambiguities can occur. Subfigure 7(b) includes a true positive example in a room without the presence of depth ambiguities and in subfigure 7(c) are a true positive and a false positive example visible, where the false positive example is influenced by depth ambiguity.

shows the excellent usage of the LDA combination of depth similarity and gradient features for human detection in depth images.

6 CONCLUSIONS

To reduce the complexity of the RDSF calculation and to keep the performance just by usage of mean and variance features on the depth image, delivers not sufficiently accurate results. The computational time of the MV-RDSF is very fast, but the accuracy of the original RDSF cannot be reached. Since, the feature space of the MV-RDSF is not significantly enough to separate the dataset, a LDA combination between the classical HOG feature and the MV-RDSF shows very good attributes to solve the problem. The time complexity of the MV-HOG-RDSF is better than of the RDSF (Ikemura and Fujiyoshi, 2010) and less features are selected (needed) in the training to separate the positive examples from the negative ones. Furthermore, just the depth image, and not the intensity or the RGB image, is needed, for a good classification result. The complexity of computing the integral images and features add up to a fast classification. Based on the LDA combination, just one classifier is needed and not a decision fusion of different classifiers, which are using just one of both feature types, as it has been done in (Wang et al., 2012).

Further research could try to combine other depth features with each other to reach more and more the best possible classification result. Still on focus should be the time complexity of the used features to produce as fast as possible classifiers for real time applications, where real time means to ensure the computation of all methods inside the frame rate of the underlying sensor, in this case 33*ms*.

ACKNOWLEDGEMENT

The research of the project ”Move and See” leading to these results has received funding from the Ministry of Health, Equalities, Care and Ageing of North Rhine-Westphalia (MGEPA), Germany and the European Union.

REFERENCES

Dalal, N. and Triggs, B. (2005). Histograms of Oriented Gradients for Human Detection. In *Proceedings of the IEEE Computer Society Conference on Computer Vision and Pattern Recognition (CVPR'05)*, volume 1, pages 886–893, San Diego,California,USA.

Dollár, P., Wojek, C., Schiele, B., and Perona, P. (2012). Pedestrian Detection: An Evaluation of the State of the Art. *IEEE Transactions on Pattern Analysis and Machine Learning*, 34(4):743 – 761.

Enzweiler, M. and Gavrila, D. M. (2009). Monocular Pedestrian Detection: Survey and Experiments. *IEEE Transactions on Pattern Analysis and Machine Intelligence*, 31(12):2179 – 2195.

Ikemura, S. and Fujiyoshi, H. (2010). Real-Time Human Detection using Relational Depth Similarity Features. In *Proceedings of the 10th Asian Conference on Computer Vision (ACCV'10)*, pages 25 – 38, Queenstown,New Zealand.

Izenman, A. J. (2008). *Modern Multivariate Statistical Techniques - Regression, Classification, and Manifold Learning*. Springer New York.

Keller, C. G., Enzweiler, M., and Gavrila, D. M. (2011). A New Benchmark for Stereo-Based Pedestrian Detection. In *IEEE Intelligent Vehicles Symposium (IV'11)*, pages 691 – 696, Baden-Baden,Germany.

Mattheij, R., Postma, E., van den Hurk, Y., and Spronck, P. (2012). Depth-based detection using haar-like features. In *Proceedings of the 24th BENELUX Conference on Artificial Intelligence (BNAIC'12)*, pages 162 – 169, Maastricht,Netherlands.

Nunn, C., Müller, D., Meuter, M., Müller-Schneiders, S., and Kummert, A. (2009). An Improved Adaboost Learning Scheme using Lda Features for Object Recognition. In *Proceedings of the 12th International IEEE Conference on Intelligent Transportation Systems (ITSC'09)*, pages 486 – 491, St. Louis,MO,USA.

Shafait, F., Keysers, D., and Breuel, T. M. (2008). Efficient Implementation of Local Adaptive Thresholding Techniques Using Integral Images. In Yanikoglu, B. A. and Berkner, K., editors, *Proceedings SPIE 6815,Document Recognition and Retrieval XV*.

Spinello, L. and Arras, K. O. (2011). People detection in RGB-D data. In *Proceedings of the IEEE/RSJ International Conference on Intelligent Robots and Systems (IROS'11)*, pages 3838 – 3843, San Francisco,CA,USA.

Viola, P. and Jones, M. (2001a). Fast and Robust Classification using Asymmetric AdaBoost and a Detector Cascade. In *Advances in Neural Information Processing System 14*, pages 1311 – 1318. MIT Press.

Viola, P. and Jones, M. (2001b). Rapid Object Detection Using a Boosted Cascade of Simple Features. In *Proceedings of the IEEE Computer Society Conference on Computer Vision and Pattern Recognition (CVPR'01)*, volume 1, pages 511 – 518, Kauai,HI,USA.

Wang, N., Gong, X., and Liu, J. (2012). A New Depth Descriptor for Pedestrian Detection in RGB-D Images. In *Proceedings of the 21st International Conference on Pattern Recognition (ICPR'12)*, pages 3688 – 3691, Tsukuba,Japan.

Wu, S., Yu, S., and Chen, W. (2011). An attempt to pedestrian detection in depth images. In *Proccedings of the 3rd Chinese Conference on Intelligent Visual Surveillance (IVS'11)*, pages 97 – 100, Beijing,China.